Published in final edited form as:
Brain Res. 2011 February 16; 1374: 63–72. doi:10.1016/j.brainres.2010.12.035.

Infraslow EEG oscillations organize large-scale cortical-subcortical interactions during sleep: a combined EEG/fMRI study

Dante Picchioni[a,*], **Silvina G. Horovitz**[b], **Masaki Fukunaga**[b], **Walter S. Carr**[c], **Jed A. Meltzer**[c], **Thomas J. Balkin**[a], **Jeff H. Duyn**[b], and **Allen R. Braun**[c]

[a] Department of Behavioral Biology, Walter Reed Army Institute of Research, Silver Spring, Maryland 20910, USA

[b] National Institute of Neurological Disorders and Stroke, National Institutes of Health, Bethesda, Maryland 20892, USA

[c] National Institute on Deafness and Other Communication Disorders, National Institutes of Health, Bethesda, Maryland 20892, USA

Abstract

Infraslow (< 0.1 Hz) oscillations of brain activity, measured by EEG and other methods, have become a subject of increasing interest. While their prominence during sleep has been established, the functional significance of these oscillations for sleep physiology is unknown. To clarify this role, we examined correlations between infraslow EEG oscillations and BOLD fMRI during the course of natural sleep in healthy volunteers. Infraslow EEG oscillations appear to organize a broad dissociation of activity in cortical and subcortical regions: in general, correlations between power in the infraslow EEG band and BOLD were positive in subcortical regions and negative in the cortex. Robust negative correlations were found principally in paramedian heteromodal cortices whereas positive correlations were seen in cerebellum, thalamus, basal ganglia, lateral neocortices and hippocampus. This pattern of correlations suggests a mechanism by which infraslow oscillations may organize sleep-dependent neuroplastic processes including consolidation of episodic memory.

Keywords

biological rhythms and sleep; cortical oscillations; EEG; fMRI; systems consolidation

1. Introduction

Rhythmic oscillations in activity appear to be one of the hallmarks of brain physiology and are central to the way the brain processes information. Electroencephalographic (EEG) oscillations have become particularly important in defining sleep stages, where frequencies below 4.0 Hz typically dominate the deeper stages of non-Rapid Eye Movement (non-REM)

[*]Corresponding author. Department of Behavioral Biology, Division of Psychiatry and Neuroscience, Walter Reed Army Institute of Research, 503 Robert Grant Ave, Silver Spring, MD 20910, USA. Phone: +1 301 319 3106. Fax: +1 301 319 9979. dante.picchioni@amedd.army.mil (D. Picchioni).

sleep. This broad range of slow frequencies actually consists of a family of oscillations (delta, slow, and infraslow), each of which may play a unique role in the physiology of sleep.

EEG oscillations during sleep that range from approximately 1.0–3.9 Hz are typically called delta oscillations, and were the first marker of sleep depth (Blake and Gerard, 1937) and sleep homeostasis (Borbely et al., 1981; Dijk and Beersma, 1989). Distinct from delta oscillations, EEG oscillations ranging from approximately 0.1–0.9 Hz are commonly called slow oscillations. Slow oscillations have a unique cellular mechanism (Steriade et al., 1993a) and may synchronize other sleep-related oscillations (Molle et al., 2002, 2006; Steriade et al., 1993b).

EEG oscillations with frequencies below 0.1 Hz are commonly called infraslow oscillations (Vanhatalo et al., 2004). The prominence of these oscillations during sleep has been demonstrated by several methods, including alternating-current EEG (Achermann and Borbely, 1997), direct-current EEG (Vanhatalo et al., 2004), multi-unit activity (Moiseeva and Aleksanian, 1986), and local field potentials (Nir et al., 2008), but their role in the physiology of sleep is poorly understood. It is believed that these EEG oscillations are well-suited to coordinate activity across large corticocortical networks (Buzsaki, 2006) and that they could, in this way, organize sleep-dependent neuroplastic processes such as the consolidation of episodic memory.

Rhythmic oscillations in brain activity below 0.1 Hz have also been observed in the blood oxygen level dependent functional magnetic resonance imaging (fMRI) signal (Biswal et al., 1995). The coherence of these fMRI oscillations has been used to identify functionally connected resting-state networks (Greicius et al., 2003), the most prominent of which is the default-mode network (Raichle et al., 2001). The precise role played by the default-mode network during wakefulness is unclear, but functions as divergent as vigilance, interoceptive cognition, and autobiographical memory have been attributed to it (Gusnard and Raichle, 2001). Recently, this network has been studied during sleep (Horovitz et al., 2008, 2009; Larson-Prior et al., 2009), but its role here remains equally obscure.

Previous studies have used hemodynamic activity measured with fMRI or positron emission tomography (PET) to characterize regional brain activity associated with specific EEG frequencies during sleep. For example, there are negative correlations between 1.5–4.0 Hz EEG oscillations and PET-based brain activity in several brainstem, diencephalic, and forebrain regions (Hofle et al., 1997; Dang-Vu et al., 2005). That is, as delta power increases, activity in these regions appears to decrease. There are also negative correlations between 0.66-0.99 Hz EEG activity and fMRI-based brain activity in several posterior cortical regions and in the thalamus (Horovitz et al., 2007).

In contrast, there are no studies of the functional neuroimaging correlates of EEG activity below 0.1 Hz, during either wakefulness or sleep. Examining the connection between the entire family of infraslow EEG oscillations and functional brain activity indexed by BOLD fMRI may provide clues as to the role played by these oscillations during sleep. In the present study, therefore, simultaneous EEG-fMRI was used to characterize the correlation between the fMRI signal and spectral power at infraslow (0.05-0.099 Hz) EEG frequencies during sleep. These correlations were compared to correlations between the fMRI signal and other members of the family of slow EEG oscillations that are prominent during sleep (0.66–0.99 and 1.0–3.9). All three correlations were entered into a conjunction analysis to assess the brain regions in which the fMRI signal was uniquely correlated with the infraslow frequency.

2. Results

Gradient and ballistocardiographic artifacts were removed from the EEG signal that was acquired simultaneously with fMRI (Fig. 1a). EEG data from these scans were sleep scored according to standard criteria (with slight modifications, see Methods section). Data from 22 scans (14 participants) were assessed and omitted from the final analysis if there were other major artifacts in the EEG (after fMRI artifact correction) or the scan did not contain stage 3 or 4 sleep. This yielded six usable scans from six separate participants. The EEG sleep stage that was most abundant during these scans was sleep stage 2, followed by 3 and then 4 (Table 1). The average length of the scans was 93 ± 54 minutes.

To measure 0.05-0.099 Hz oscillations, a spectral analysis was performed using a 45-second moving window. The same window was used for the spectral analysis of 0.66–0.99 and 1.0–3.9 Hz oscillations so that window length would not be a potential source of power differences. Activity from 0.1–0.659 Hz was not assessed because there was respiratory artifact in the EEG signal that peaked at approximately 0.3 Hz. In contrast to the typical increases in 1.0–3.9 and 0.66–0.99 Hz activity that are seen during stages 3 and 4 sleep, spectral power at 0.05–0.099 Hz fluctuated in a novel manner across these and other sleep stages: there was greater variability in this signal and there were intermittent peaks during the transition between the first and second non-REM period (Fig. 1b).

The fMRI data were temporally smoothed using a window that matched the length and filter kernel of the window used in the EEG spectral analysis. Each of the three EEG oscillations was modeled separately on a volume-by-volume basis in a parametric design yielding three sets of EEG-fMRI correlations across all sleep stages. To identify the unique features of correlations with the infraslow frequency band, a conjunction analysis was performed that classified each voxel into one of 27 mutually exclusive and logically exhaustive categories. These categories were based on the appropriate inclusive and exclusive Boolean combinations of significant, non-significant, positive, and negative correlations between the three oscillations.

The binary, three-dimensional image maps from the conjunction categories that represented the unique correlations for infraslow oscillations (significant positive or negative correlation for that oscillation and a non-significant correlation for the other two oscillations) were used to mask the continuous *t* values from the original bivariate correlations. Results of these masking procedures are displayed in Figures 2-4. The coordinates of the local maxima for the clusters of significant 0.05–0.099 Hz correlations are displayed in Tables 2 and 3. Clusters less than 100 voxels are excluded, with exceptions (especially for small regions such as the thalamus) noted in the legend.

Correlations between the fMRI signal and power in the infraslow band were characterized by a conspicuous anatomical dissociation: correlations with cortical regions were generally positive and correlations with subcortical regions were generally negative, as is evident in Fig. 2. Negative correlations were strongest and most abundant in heteromodal cortices along the midline. That is, anteriorly in medial and superior frontal gyri, SMA and anterior cingulate cortex and posteriorly in retrosplenial cortex, posterior cingulate cortex, and precuneus (Fig. 2, Table 2). Negative correlations were also found in lateral cortical areas as well. The majority of these were again in heteromodal areas (middle and inferior frontal, middle temporal gyri), but were also detected in unimodal cortices (pre- and postcentral, middle occipital gyri) (Fig. 3, Table 2). Positive correlations with subcortical structures were found in the thalamus (anterior, medial and ventrolateral nuclei), basal ganglia (globus pallidus, caudate, and putamen), and brainstem (dorsal mesencephalon). Widespread positive correlations between infraslow oscillations and fMRI activity included the

cerebellum (Fig. 2, Table 3) as well. Some positive correlations were also seen in the neocortex. Except for the medial orbital cortices, these were found exclusively in lateral rather than paramedian areas and included both unimodal (postcentral gyrus, inferior temporal, lingual, fusiform gyri; superior temporal gyrus) and heteromodal cortices (supramarginal, inferior frontal and middle temporal gyri, temporal pole) (Fig. 3, Table 3). Importantly, infraslow oscillations were also positively correlated with activity in the hippocampus and parahippocampal gyri (Fig. 4, Table 3).

3. Discussion

Previous studies of slow EEG oscillations during sleep have been complicated by inconsistencies in nomenclature. For example, slow oscillations (i.e., 0.1–0.9 Hz) have sometimes been defined with bandwidth limits that resulted in an overlap with 1.0–3.9 Hz oscillations (e.g., Dang-Vu et al., 2008). Some of this confusion may be due to the fact that 0.5–1.9 Hz "slow waves" are used to visually score stages 3 and 4 sleep (Rechtschaffen and Kales, 1968). It is, however, clear from cellular recordings in animals that these frequency bands have distinct features (Steriade et al., 1993a, 1993b) and therefore, should be analyzed separately. And it may be particularly important to evaluate the infraslow oscillations independently. First, this frequency band may be unique in providing a physiological mechanism by which activity is correlated across large-scale cortical networks during sleep. Second, although slow oscillations and delta oscillations vary systematically with sleep stage (indeed, their abundance is used to define the deeper stages of sleep), infraslow oscillations do not. Instead, they vary independently of the other frequencies and are prominent in all stages of sleep. Therefore, while previous studies have often failed to discriminate between frequencies greater or less than 0.1 Hz, and have typically restricted the analysis to a particular stage of sleep, the present study was designed to differentiate activity in discrete slow EEG frequency bands across all sleep stages.

The three bands of interest—delta (1.0–3.9 Hz), slow (0.1–0.9 Hz), and infraslow oscillations (< 0.1 Hz)—were measured using a moving spectral analysis window and correlated with fMRI activity that was temporally smoothed using the same window length and filter kernel. A conjunction analysis was then performed to identify the unique correlations between infraslow EEG activity and fMRI activity. The results indeed revealed widespread patterns of correlation that were exclusively related to the infraslow band.

3.1. Patterns of anatomical dissociation

A striking finding was the near-complete segregation of positive and negative correlations between infraslow oscillations and activity in subcortical and cortical brain areas: as power in the infraslow band increased, activity in subcortical regions tended to increase, whereas activity decreased in the cortex. This reciprocal pattern can be interpreted in a number of ways.

A dissociated pattern of cortical and subcortical activity may itself be characteristic of states of decreased consciousness (Hamandi et al., 2006), and has been reported in some (Goldman et al., 2002; Moosmann et al., 2003; Feige et al., 2005)—though not all (Laufs et al., 2003)—studies that correlated fMRI activity with alpha EEG oscillations, which are associated with the drowsiness, inattention, and decreasing levels of consciousness occurring immediately prior to sleep onset. The same pattern of EEG-fMRI correlations is also observed when comparing EEG periods with and without absence seizures (e.g., Gotman et al., 2005; Hamandi et al., 2006; Moeller et al., 2008). Absence seizures are characterized by impaired consciousness and appear to be regulated by the same thalamocortical mechanisms that regulate the sleep-wake cycle (Steriade, 2005).

The reciprocal pattern of correlations between fMRI activity and infraslow oscillations may be related to the mechanisms by which infraslow oscillations are generated. Nonspecific thalamic nuclei relay signals from the midbrain-pontine reticular formation to the cortex and activity relayed in this way appears to regulate cortical arousal (Steriade and McCarley, 2005). These nonspecific thalamic nuclei are located in the intralaminar regions of the thalamus, including its medial regions. In the present study, the positive correlations with infraslow oscillations in the medial thalamus (see Table 2) could be related to the generation of infraslow oscillations through these nonspecific nuclei. That is, opposing thalamic and neocortical correlations may reflect a reciprocal interaction between the thalamus and the cortex, which may be fundamentally related to the generation of thalamocortical oscillations (Gotman et al., 2005).

There was also a similar dissociation between infraslow oscillations and activity in lateral and medial forebrain regions: correlations with infraslow oscillations were in general positive in lateral areas and negative in medial areas. This roughly parallels a theoretical distinction that proposes two widespread, functionally divergent brain systems: a medial, archicortically-derived system that plays a role in internally generated, self-motivated behaviors, and a lateral, paleocortically-derived system that is more responsive to extroceptive stimuli (Goldberg, 1985). This account suggests that a functional dissociation between interoceptive and exteroceptive mechanisms may be driven by infraslow oscillations during sleep.

3.2. Reciprocal correlations in the default mode network

Another way to approach the present findings is to examine fMRI correlations of infraslow oscillations with regions of the default-mode network. This system, consisting of paramedian frontal, parietal and cingulate, inferior parietal, lateral temporal and parahippocampal/hippocampal cortices, was first described by Raichle and colleagues (Raichle et al., 2001) as the baseline state of the brain, reflecting intrinsic brain activity during the resting state. Interestingly, another way the default-mode network has been defined is by coherent fluctuations of the fMRI signal in the same frequency range as the infraslow EEG oscillations evaluated here (Greicius et al., 2003). Most importantly, as noted above, the integrity of the DMN has been actively investigated during sleep (Horovitz et al. 2008, 2009; Larson-Prior et al., 2009).

An earlier notion—that the integrity of the default-mode network is stable throughout wakefulness, sleep, and other altered states of consciousness (Vincent et al., 2007)—has been modified by the finding that, while stable in stage 1 and 2 sleep (Larson-Prior et al., 2009), its integrity is altered in stage 3 and 4 sleep (Horovitz et al., 2009). That is, functional connections between anterior and posterior nodes of the default-mode network appear to be attenuated during sleep stages characterized by slower oscillations. In the present study, we detected a different pattern of uncoupling within this network, explicitly associated with oscillations in the infraslow range: negative correlations with activity in regions that constitute the paramedian nodes of the default-mode network (medial prefrontal/anterior cingulate, precuneus, and posterior cingluate and retrosplenial cortices) and positive correlations with activity in regions that constitute its prominent neocortical and allocortical nodes (inferior parietal lobule, lateral temporal cortex and, crucially, hippocampus and parahippocampal gyri).

Another interpretation of this pattern, which is observed during all sleep stages, is that infraslow oscillations may be important for the sleep-dependent consolidation of episodic memories. During wakefulness, a potential function of default-mode network activity is to support the retrieval of autobiographical memories (Buckner et al., 2008; Vincent et al., 2006). According to current models, the storage of long-term memories in a corticocortical

network requires a selective strengthening between the nodes in that network during sleep so the memories can become independent of their representation in the hippocampus (Frankland and Bontempi, 2005). Default-mode network regions may play a role in this process: crucially, it has been shown that activity in the default-mode network is increasingly associated with correct recognition of stimuli on an episodic memory task whereas activity in the hippocampus is decreasingly associated with correct recognition (Takashima et al., 2007, 2006). The present data suggest a mechanism by which a sleep-dependent transfer of mnemonic information from hippocampus to neocortex may occur. Infraslow oscillations, by organizing the coordinated, reciprocal activity in the hippocampal and neocortical elements of the default-mode network, may lead to an associated Hebbian strengthening of the cortical connections that support systems-level consolidation (Balduzzi et al., 2008).

3.3. Limitations

The participants in this study were sleep deprived in order to facilitate sleep inside the scanner. Sleep following sleep deprivation is known to be different from sleep following a single day of wakefulness. Although it is unlikely this affected the basic relationships observed in the present study, future sleep fMRI studies should be designed to measure brain activity following a single day of wakefulness. Another limitation of the present study is the relatively small sample size ($n = 6$).

3.4 Conclusion

Additional work will be needed to specifically address the hypothesis regarding systems-level consolidation, since the present study did not compare cognitive measures before and after the intervening period of sleep. In order to address the functional significance of EEG and fMRI-based brain activity during sleep, future studies will need to correlate it with overnight improvements in a cognitive task, specifically those indexing the consolidation of episodic memories. This will allow a more complete evaluation of the relationship between brain activity during sleep and sleep-dependent learning and should shed additional light on the roles played by neocortical oscillations in sleep-dependent neuroplasticity.

4. Experimental Procedure

4.1. Participants and procedure

Procedures were approved by Institutional Review Boards at the Walter Reed Army Institute of Research and the National Institutes of Health. The research was carried out in accordance with The Code of Ethics of the World Medical Association (Declaration of Helsinki). All participants gave written informed consent and were monetarily compensated. All participants were right handed, were fluent English speakers, were not pregnant, consumed less than 24 oz of caffeinated beverages per day (8.1 ± 7.4 oz), were non-tobacco users, did not use any illicit drugs, were not extreme morning or evening types, did not engage in any shift work for 12 months before the study, were free of a history or current diagnosis of psychological or neurological disorders as assessed by an interview and a neurological examination, were free of auditory abnormalities as assessed by a clinical audiological examination, and were free of sleep disorders as assessed using a custom questionnaire and a standard clinical nocturnal polysomnogram. Sleep was also monitored at home with wrist-worn actigraphs (Ambulatory Monitoring, Inc., Ardlsey, USA) for seven days prior to the study to ensure a regular sleep routine with adequate amounts of sleep.

To facilitate sleep inside the scanner, participants underwent approximately 44 hours of total sleep deprivation where they were under near-constant supervision and were not allowed any stimulants. Participants were scanned at 02:30. The scanning period lasted for a

maximum of three hours with the possibility of multiple scans in this period. Data from 22 scans (14 participants) were assessed and omitted from the final analysis if there were other major artifacts in the EEG (after fMRI artifact correction) or the scan did not contain stage 3 or 4 sleep. If a participant had more than one scan with stage 3 or 4 sleep, the scan with more sleep was chosen. This yielded six (6) usable scans from separate participants. These participants were 23.6 ± 1.8 years old and there were two (2) males.

4.2. EEG acquisition

Data were acquired using MRI-compatible hardware and the associated software (Brain Products, GmbH, Gilching, Germany). This included the alternating-current amplifier (BrainAmp MR Plus), the direct-current amplifier (BrainAmp ExG MR), and sintered silver-silver chloride ring electrodes with carbon fibers (BrainCap MR). A total of 16 channels were collected using the alternating-current amplifier at 5 kHz. These included 14 EEG locations (FP_1, FP_2, F_Z, FC_5, FC_6, C_3, C_4, C_Z, P_Z, TP_9, TP_{10}, O_1, O_2, O_Z) and a single channel each for electro-oculography and electrocardiography. All electrodes were programmed to use FC_Z as the recording reference and a location near C_Z as the ground. This amplifier is designed with an alternating current-coupling passive resistor-capacitor 0.016 Hz high-pass analog filter (6 decibels/octave) and a Butterworth 250 Hz low-pass analog filter (30 decibels/octave). Using a separate set of simulated data, there was no indication of residual attenuation at 0.05 Hz due to the roll-off characteristics of the high-pass filter. Chin electromyographic data were collected with the direct-current amplifier. Acquisition software was Recorder.

4.3. EEG processing

fMRI gradient field switching and static field ballistocardiographic artifacts were removed using routines in Analyzer. These routines are based on standard approaches for EEG data collected during fMRI (Allen et al., 2000; Srivastava et al., 2005). All subsequent EEG data processing was also performed using Analyzer.

Sleep scoring was performed on data with standard software filters and according to standard criteria (Rechtschaffen and Kales, 1968) with slight modifications noted below. This included a band-pass filter of 0.5-20.0 Hz for the EEG and electro-oculographic channels and a high-pass filter of 10 Hz and a low-pass filter of 70 Hz with a notch filter at 60 Hz for the electromyographic channel. Sleep scoring was performed from C_3 with a P_3 reference rather than the standard A_2 reference because the latter caused an unusually high amplification of the signals due to the static magnetic field. Records were scored in 12-second epochs rather than the standard 30-second epochs to maximize temporal resolution. That is, sleep was scored in 12-second epochs so there would only be 4 image repetitions per sleep epoch rather than 10 image repetitions. All records were sleep scored by an experienced polysomnographic technologist (D.P.). An independent assessment of inter-rater reliability for a representative record was performed between this scorer and a Diplomate of the American Board of Sleep Medicine (T.J.B.). The agreement was 73%. This is as good as could be expected considering the technical difficulties of acquiring simultaneous EEG and fMRI data.

Spectral analysis (fast Fourier transformation) was performed on data without any software filters, which necessitated rejecting any records with significant low-frequency artifact. Prior to the spectral analysis, data from the 14 scalp channels were averaged (malfunctioning channels were removed prior to averaging). This is equivalent to analyzing data from FC_Z (the recording reference) with an average (re)reference.

To measure activity in the 0.05–0.099 Hz band, a spectral analysis was performed using a 45-second moving Hamming window. The window was advanced in 3-second increments to match the fMRI repetition time. The same 45-second window was used for the spectral analysis of 0.66–0.99 and 1.0–3.9 Hz oscillations so that window length would not be a potential source of power differences. Preliminary analyses revealed little difference between using this large window and a more conventional 3-second non-overlapping window for calculating the spectral power for these two faster oscillations. Activity from 0.1–0.659 Hz was not analyzed because there was respiratory artifact in the EEG signal (likely due to the static magnetic field) that peaked at approximately 0.3 Hz. Smoothed spectral power (1st-degree negative exponential smoother with rejection of outliers) was used to create the figure of EEG spectral power across time because overlap in the fluctuations obscured the overall trend of the individual bands. Raw (i.e., unsmoothed) EEG spectral power was used in the correlations with fMRI activity.

4.4. fMRI acquisition

MRI data was acquired on a 3T scanner (GE, Milwaukee, USA). For the functional scans, a 16-channel receive-only detector array was used (de Zwart et al., 2004). This array is designed with a helmet-type construction that minimizes the distance between the individual coils and the scalp as a tradeoff for slight signal dropout in the lower cerebellum and brain stem. The coil was foam-padded to limit head motion and improve participant comfort. A foam mattress pad was placed on the scanner table to improve participant comfort. Blood oxygen level dependence fMRI was implemented using an echo planar imaging sequence. This was preceded by a short functional run that included 10 different echo times, to be used as a reference for correction of geometric distortions. Both functional runs included 25 axial slices (3.45 x 3.45 mm^2 nominal in-plane resolution, 4.5 mm thickness, 0.5 mm gap). Other parameters were as follows: repetition time = 3 s, echo time = 45 ms, flip angle = 90°, and a maximum of 3600 image repetitions. To facilitate sleep, the acoustic noise generated by the functional sequence was kept below a sound pressure level of 96 decibels by decreasing the bandwidth to 62.54 kHz and limiting the gradient slew-rate to 25 T/m/s. Participants also wore earplugs.

T2-weighted anatomical images (fast spin echo) were collected for geometric distortion correction. If the session was interrupted and the participant agreed to continue, additional T2-weighted anatomical images were acquired to correct for the new head position. Respiratory effort was measured using a strain gauge on the abdomen and cardiac rate was measured using an infrared pulse oximeter on a finger. Both transducers were standard equipment on the MRI scanner and the data were collected using custom software at a frequency of 1 kHz.

4.5. fMRI processing

Data were pre-processed using custom routines written in IDL (ITT Visual Information Solutions, Inc., Boulder, USA) unless otherwise indicated. Slice timing correction was applied. Motion correction was applied by registering the functional data to the first image of the short functional run. Both corrections were performed using SPM2 software (Wellcome Department of Cognitive Neurology, London, UK). Distortion correction was performed using the field map computed from the 10 different echo times of the short functional run (Jezzard et al., 1995). This correction was necessary due to the geometric distortions that were caused by the low bandwidth needed to decrease the acoustic noise. Remaining distortion was corrected by nonlinearly deforming the functional data to match the undistorted T2-weighted anatomical images using AIR 5.2.5 software (University of California, Los Angeles, Los Angeles, USA). Physiological noise was corrected by modeling the cardiac rate, respiratory rate, and respiratory envelope and regressing out the

activity associated with these variables (Glover et al., 2000; Shmueli et al., 2007). Global signal correction was applied using the within-volume mean as a linear regression covariate. A high-pass filter (0.005 Hz) was applied to remove any baseline drifts.

The following additional processing steps were performed with AFNI (National Institute of Mental Health, Bethesda, USA). This included masking functional activity outside the brain, transforming the functional data to Talairach space using a standardized template (Wellcome Department of Cognitive Neurology, London, UK) with a final voxel size of 1.0 mm^3, Gaussian spatial blurring (4 mm), and temporal smoothing. The temporal smoothing was programmed to use a 45-second Hamming window (matching the window length and filter kernel from the EEG spectral analysis). This was performed so that each time point in the subsequent correlation analysis would be based on data from the same temporal range in each modality. This smoothing could be considered equivalent to applying a low-pass filter at approximately 0.02 Hz. Although this might reduce the ability to measure the coherence between oscillations in the EEG and fMRI signal, this study was interested in the correlations between spectral power in the EEG and the raw fMRI signal intensity.

4.6. Statistical analysis

All statistical analyses were performed with AFNI (National Institute of Mental Health, Bethesda, USA). Zero padding was added to the beginning and end of the EEG spectral analysis timing files to account for the missing data associated with the periods where the 45-second spectral analysis window was not fully immersed in the data. These volumes were also censored from the EEG-fMRI correlations. The timing files associated with the spontaneous, volume-by-volume fluctuations of EEG spectral activity for the three oscillations were convolved with a canonical hemodynamic response function (delay time = 2 s, rise time = 4 s, fall time = 6 s, undershoot/peak ratio = 0.2, undershoot restore time = 2 s).

The analysis was performed according to a standard two-level approach at the individual participant and group level. Each oscillation was modeled separately on a volume-by-volume basis in a parametric design yielding three sets of EEG-fMRI correlations (ultimately to be subjected to a conjunction analysis to assess unique effects). Given that sleep scoring itself is based on the relative presence of various oscillations, the analysis was conducted across the entire scan regardless of sleep stage. This allowed the volume-by-volume variability in spectral power to determine the results directly, rather than imposing tautological pre-constraints with sleep scoring, which would have restricted the range of spectral power across the sleep period. Such an approach is consistent with findings of EEG spectral power differences (Borbely et al., 1981) and fMRI differences (Picchioni et al., 2008) *within* the discontinuous sleep stages.

Data were corrected for multiple comparisons using a False Discovery Rate (corrected $p < 0.05$ across the whole brain), which controls the proportion of false positives (Logan and Rowe, 2004). The correlations were then transformed using the Fisher *z*-transformation in preparation for analysis at the group level. The transformed correlations were averaged across participants and tested for significance using a *t* test with a null value of zero.

To allow for the discussion of the unique effects associated with infraslow oscillations, a conjunction analysis was performed that classified each voxel into one of 27 mutually exclusive and exhaustive categories. These categories were based on the appropriate inclusive and exclusive Boolean combinations of significant ($p < 0.05$), non-significant, positive, and negative correlations between the three oscillations. The binary, three-dimensional image maps from the conjunction categories that represented the unique correlations for infraslow oscillations (significant positive or negative correlation for that

oscillation and a non-significant correlation for the other two oscillations) were used to mask the continuous *t* values from the original bivariate correlations. The data were also analyzed with partial correlations by entering the spectral power for all three bands into a multiple regression equation; the partial correlations for infraslow oscillations were nearly identical to the results from the conjunction analysis and only the results for the conjunction analysis are presented.

Coordinates in Talairach space (Left/Right, Posterior/Anterior, Inferior/Superior negative/positive convention) were determined by the center of mass within the clusters of significant voxels from the masked dataset. Clusters less than 100 voxels were excluded with exceptions (especially for small regions) noted in the table legends. Functional images are displayed on the standardized average of 27 T1-weighted scans of a single participant known as the "Colin Brain" (Montreal Neurological Institute, Montreal, Canada).

Highlights

We examined correlations between infraslow EEG oscillations and BOLD fMRI during the course of natural sleep in healthy volunteers.

Infraslow EEG oscillations appear to organize a broad dissociation of activity in cortical and subcortical regions.

Correlations between power in the infraslow EEG band and BOLD were positive in subcortical regions and negative in the cortex.

This pattern of correlations suggests a mechanism by which infraslow oscillations may organize sleep-dependent neuroplastic processes including consolidation of episodic memory.

Acknowledgments

The views expressed in this article are those of the authors and do not reflect the official policy or position of the Department of the Army, the Department of the Navy, the Department of Defense, the Department of Health and Human Services, the National Institutes of Health, the U.S. Government, or any of the institutions with which the authors are affiliated. W.S.C. is a Lieutenant Commander in the U.S. Navy and this work was prepared as part of his official duties. All of the other authors similarly performed this work as employees of the u.s. government. Title 17 U.S.C. §105 provides that 'Copyright protection under this title is not available for any work of the United States Government.' Title 17 U.S.C. §101 defines a U.S. Government work as a work prepared by a military service member or employee of the U.S. Government as part of that person's official duties.

The authors would like to thank the following individuals for their assistance with this project: Carmen Brewer, Christopher Zalewski, Alex Krugler, Kacie Smith, Teresa Kessinger, Jim Paterson, Jacco de Zwart, Peter van Gelderen, Sadat Shamim, Susumu Sato, Jackie Greenfield, Michael Duran, Ingmar Gutberlet, Natalie Villacorta, Blair Hu, Nate Coddington, and Suraji Wagage.

References

Achermann P, Borbely AA. Low-frequency (< 1 Hz) oscillations in the human sleep electroencephalogram. Neuroscience. 1997; 81:213–222. [PubMed: 9300413]

Allen PJ, Josephs O, Turner R. A method for removing imaging artifact from continuous EEG recorded during functional MRI. Neuroimage. 2000; 12:230–239. [PubMed: 10913328]

Balduzzi D, Riedner BA, Tononi G. A BOLD window into brain waves. Proc Natl Acad Sci USA. 2008; 105:15641–15642. [PubMed: 18843102]

Biswal B, Yetkin FZ, Haughton VM, Hyde JS. Functional connectivity in the motor cortex of resting human brain using echo-planar MRI. Magn Reson Med. 1995; 34:537–541. [PubMed: 8524021]

Blake H, Gerard RW. Brain potentials during sleep. Am J Physiol. 1937; 119:692–703.

Borbely AA, Strauch I, Baumann F, Brandeis D, Lehmann D. Sleep deprivation: Effect on sleep stages and EEG power density in man. Electroencephalogr Clin Neurophysiol. 1981; 51:483–493. [PubMed: 6165548]

Buckner RL, Andrews-Hanna JR, Schacter DL. The brain's default network: anatomy, function, and relevance to disease. Ann NY Acad Sci. 2008; 1124:1–38. [PubMed: 18400922]

Buzsaki, G. Rhythms of the Brain. Oxford University Press; New York: 2006.

Dang-Vu TT, Desseilles M, Laureys S, Degueldre C, Perrin F, Phillips C, Maquet P, Peigneux P. Cerebral correlates of delta waves during non-REM sleep revisited. Neuroimage. 2005; 28:14–21. [PubMed: 15979343]

Dang-Vu TT, Schabus M, Desseilles M, Albouy G, Boly M, Darsaud A, Gais S, Rauchs G, Sterpenich V, Vandewalle G, Carrier J, Moonen G, Balteau E, Degueldre C, Luxen A, Phillips C, Maquet P. Spontaneous neural activity during human slow wave sleep. Proc Natl Acad Sci USA. 2008; 105:15160–15165. [PubMed: 18815373]

de Zwart JA, Ledden PJ, van Gelderen P, Bodurka J, Chu R, Duyn JH. Signal-to-noise ratio and parallel imaging performance of a 16-channel receive-only brain coil array at 3.0 T. Magn Reson Med. 2004; 51:22–26. [PubMed: 14705041]

Dijk DJ, Beersma DG. Effects of SWS deprivation on subsequent EEG power density and spontaneous sleep duration. Electroencephalogr Clin Neurophysiol. 1989; 72:312–320. [PubMed: 2467797]

Feige B, Scheffler K, Esposito F, Di Salle F, Hennig J, Seifritz E. Cortical and subcortical correlates of electroencephalographic alpha rhythm modulation. J Neurophysiol. 2005; 93:2864–2872. [PubMed: 15601739]

Frankland PW, Bontempi B. The organization of recent and remote memories. Nat Rev Neurosci. 2005; 6:119–130. [PubMed: 15685217]

Glover GH, Li TQ, Ress D. Image-based method for retrospective correction of physiological motion effects in fMRI: RETROICOR. Magn Reson Med. 2000; 44:162–167. [PubMed: 10893535]

Goldberg G. Supplementary motor area structure and function: review and hypotheses. Behav Brain Sci. 1985; 8:567–616.

Goldman RI, Stern JM, Engel J Jr, Cohen MS. Simultaneous EEG and fMRI of the alpha rhythm. Neuroreport. 2002; 13:2487–2492. [PubMed: 12499854]

Gotman J, Grova C, Bagshaw A, Kobayashi E, Aghakhani Y, Dubeau F. Generalized epileptic discharges show thalamocortical activation and suspension of the default state of the brain. Proc Natl Acad Sci USA. 2005; 102:15236–15240. [PubMed: 16217042]

Greicius MD, Krasnow B, Reiss AL, Menon V. Functional connectivity in the resting brain: a network analysis of the default mode hypothesis. Proc Natl Acad Sci USA. 2003; 100:253–258. [PubMed: 12506194]

Gusnard DA, Raichle ME. Searching for a baseline: functional imaging and the resting human brain. Nat Rev Neurosci. 2001; 2:685–694. [PubMed: 11584306]

Hamandi K, Salek-Haddadi A, Laufs H, Liston A, Friston K, Fish DR, Duncan JS, Lemieux L. EEG-fMRI of idiopathic and secondarily generalized epilepsies. Neuroimage. 2006; 31:1700–1710. [PubMed: 16624589]

Hofle N, Paus T, Reutens D, Fiset P, Gotman J, Evans AC, Jones BE. Regional cerebral blood flow changes as a function of delta and spindle activity during slow wave sleep in humans. J Neurosci. 1997; 17:4800–4808. [PubMed: 9169538]

Horovitz SG, Braun AR, Carr WS, Picchioni D, Balkin TJ, Fukunaga M, Duyn JH. Decoupling of the brain's default mode network during deep sleep. Proc Natl Acad Sci USA. 2009; 106:11376–11381. [PubMed: 19549821]

Horovitz SG, Fukunaga M, de Zwart JA, van Gelderen P, Fulton SC, Balkin TJ, Duyn JH. Low frequency BOLD fluctuations during resting wakefulness and light sleep: a simultaneous EEG-fMRI study. Hum Brain Mapp. 2008; 29:671–682. [PubMed: 17598166]

Horovitz, SG.; Fukunaga, M.; Picchioni, D.; Carr, WS.; De Zwart, JA.; Van Gelderen, P.; Balkin, TJ.; Braun, AR.; Duyn, JH. Metabolic imprint of slow oscillations during deep sleep in humans. Oral presentation at the Society for Neuroscience meeting; San Diego, CA. 2007.

Jezzard P, Balaban RS. Correction for geometric distortion in echo planar images from B0 field variations. Magn Reson Med. 1995; 34:65–73. [PubMed: 7674900]

Larson-Prior LJ, Zempel JM, Nolan TS, Prior FW, Snyder AZ, Raichle ME. Cortical network functional connectivity in the descent to sleep. Proc Natl Acad Sci USA. 2009; 106:4489–4494. [PubMed: 19255447]

Laufs H, Kleinschmidt A, Beyerle A, Eger E, Salek-Haddadi A, Preibisch C, Krakow K. EEG-correlated fMRI of human alpha activity. Neuroimage. 2003; 19:1463–1476. [PubMed: 12948703]

Logan BR, Rowe DB. An evaluation of thresholding techniques in fMRI analysis. Neuroimage. 2004; 22:95–108. [PubMed: 15110000]

Moeller F, Siebner HR, Wolff S, Muhle H, Granert O, Jansen O, Stephani U, Siniatchkin M. Simultaneous EEG-fMRI in drug-naive children with newly diagnosed absence epilepsy. Epilepsia. 2008; 49:1510–1519. [PubMed: 18435752]

Moiseeva NI, Aleksanian ZA. Slow-wave oscillations of the multi-unit activity average frequency in the human brain during drowsiness and sleep. Electroencephalogr Clin Neurophysiol. 1986; 22:431–437. [PubMed: 2420559]

Molle M, Marshall L, Gais S, Born J. Grouping of spindle activity during slow oscillations in human non-rapid eye movement sleep. J Neurosci. 2002; 22:10941–10947. [PubMed: 12486189]

Molle M, Yeshenko O, Marshall L, Sara SJ, Born J. Hippocampal sharp wave-ripples linked to slow oscillations in rat slow-wave sleep. J Neurophysiol. 2006; 22:62–70. [PubMed: 16611848]

Moosmann M, Ritter P, Krastel I, Brink A, Thees S, Blankenburg F, Taskin B, Obrig H, Villringer A. Correlates of alpha rhythm in functional magnetic resonance imaging and near infrared spectroscopy. Neuroimage. 2003; 20:145–158. [PubMed: 14527577]

Nir Y, Mukamel R, Dinstein I, Privman E, Harel M, Fisch L, Gelbard-Sagiv H, Kipervasser S, Andelman F, Neufeld MY, Kramer U, Arieli A, Fried I, Malach R. Interhemispheric correlations of slow spontaneous neuronal fluctuations revealed in human sensory cortex. Nat Neurosci. 2008; 11:1100–1108. [PubMed: 19160509]

Picchioni D, Fukunaga M, Carr WS, Braun AR, Balkin TJ, Duyn JH, Horovitz SG. fMRI differences between early and late stage-1 sleep. Neurosci Lett. 2008; 441:81–85. [PubMed: 18584959]

Raichle ME, MacLeod AM, Snyder AZ, Powers WJ, Gusnard DA, Shulman GL. A default mode of brain function. Proc Natl Acad Sci USA. 2001; 98:676–682. [PubMed: 11209064]

Rechtschaffen, A.; Kales, A. A Manual of Standardized Terminology, Techniques, and Scoring System for Sleep Stages of Human Subjects. Brain Research Institute; Los Angeles: 1968.

Shmueli K, van Gelderen P, de Zwart JA, Horovitz SG, Fukunaga M, Jansma JM, Duyn JH. Low-frequency fluctuations in the cardiac rate as a source of variance in the resting-state fMRI BOLD signal. Neuroimage. 2007; 38:306–320. [PubMed: 17869543]

Srivastava G, Crottaz-Herbette S, Lau KM, Glover GH, Menon V. ICA-based procedures for removing ballistocardiogram artifacts from EEG data acquired in the MRI scanner. Neuroimage. 2005; 24:50–60. [PubMed: 15588596]

Steriade M. Sleep, epilepsy and thalamic reticular inhibitory neurons. Trends Neurosci. 2005; 28:317–324. [PubMed: 15927688]

Steriade, M.; McCarley, R. Brain control of wakefulness and sleep. 2. Brain Springer-Verlag; New York: 2005.

Steriade M, Nunez A, Amzica F. A novel slow (< 1 Hz) oscillation of neocortical neurons in vivo: depolarizing and hyperpolarizing components. J Neurosci. 1993a; 13:3252–3265. [PubMed: 8340806]

Steriade M, Nunez A, Amzica F. Intracellular analysis of relations between the slow (< 1 Hz) neocortical oscillation and other sleep rhythms of the electroencephalogram. J Neurosci. 1993b; 13:3266–3283. [PubMed: 8340807]

Takashima A, Petersson KM, Rutters F, Tendolkar I, Jensen O, Zwarts MJ, McNaughton BL, Fernandez G. Declarative memory consolidation in humans: a prospective functional magnetic resonance imaging study. Proc Natl Acad Sci USA. 2006; 103:756–761. [PubMed: 16407110]

Takashima A, Nieuwenhuis IL, Rijpkema M, Petersson KM, Jensen O, Fernández G. Memory trace stabilization leads to large-scale changes in the retrieval network: a functional MRI study on associative memory. Learn Mem. 2007; 14:472–479. [PubMed: 17622649]

Vanhatalo S, Palva JM, Holmes MD, Miller JW, Voipio J, Kaila K. Infraslow oscillations modulate excitability and interictal epileptic activity in the human cortex during sleep. Proc Natl Acad Sci USA. 2004; 101:5053–5057. [PubMed: 15044698]

Vincent JL, Patel GH, Fox MD, Snyder AZ, Baker JT, Van Essen DC, Zempel JM, Snyder LH, Corbetta M, Raichle ME. Intrinsic functional architecture in the anaesthetized monkey brain. Nature. 2007; 447:83–86. [PubMed: 17476267]

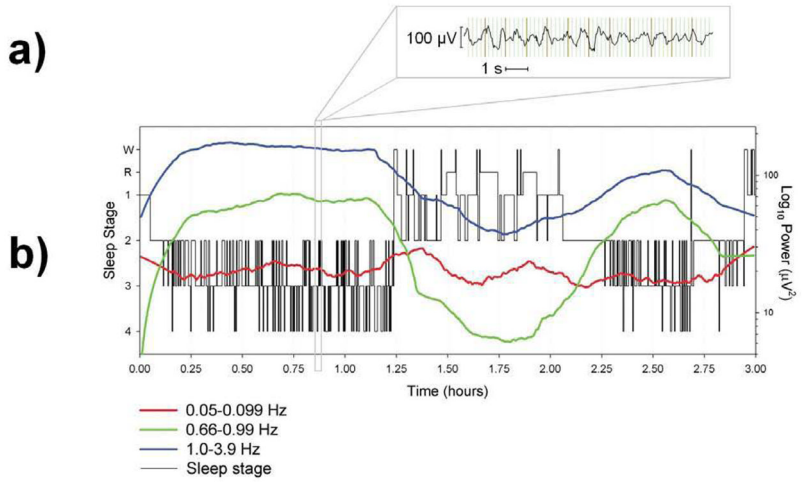

Fig. 1.

EEG results from one participant who slept for the maximum duration of three hours during a single scan. a) Example of a 12-second epoch of EEG during sleep stage 4 after fMRI gradient and ballistocardiographic artifact removal. b) Sleep scoring (left axis) and spectral power (right axis) for the three oscillations under investigation. Spectral power data are smoothed using a negative exponential (1st degree) smoother with rejection of outliers. Smoothed spectral power was used to create this figure because overlap in the fluctuations obscured the overall trend of the individual bands. Raw (i.e., unsmoothed) EEG spectral power was used in the correlations with fMRI activity. W = Wakefulness and R = REM.

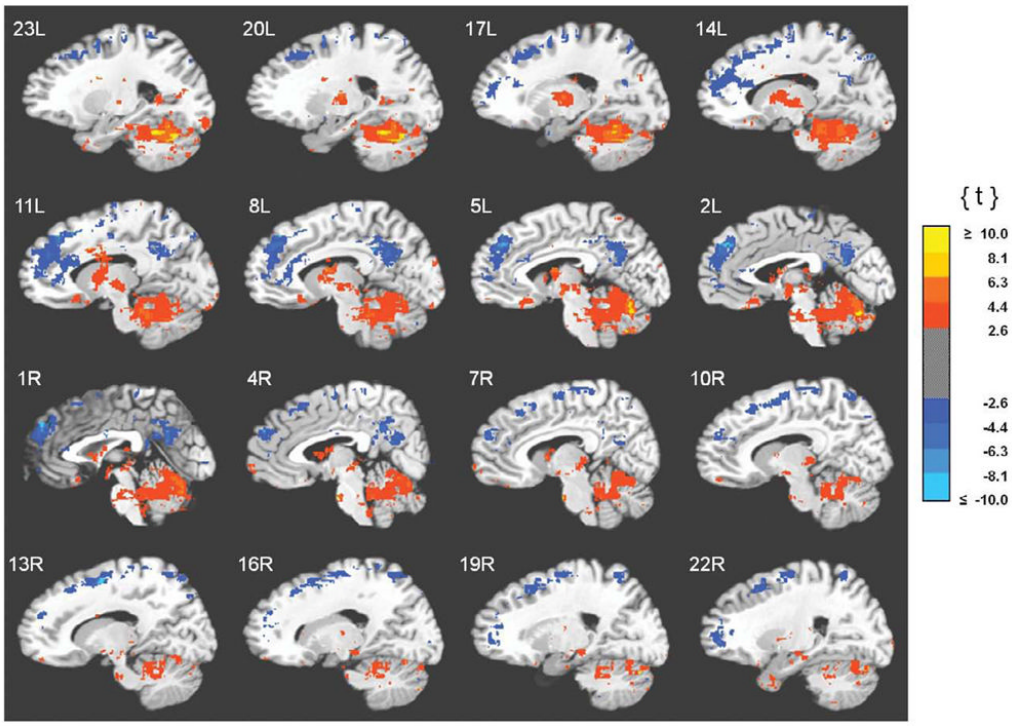

Fig. 2.

Clusters of unique correlations between fMRI activity and 0.05–0.099 Hz EEG spectral power. Functional images are displayed on the standardized average of 27 T1-weighted scans of a single participant known as the "Colin Brain" (Montreal Neurological Institute, Montreal, Canada). Voxel size is 1.0 mm^3.

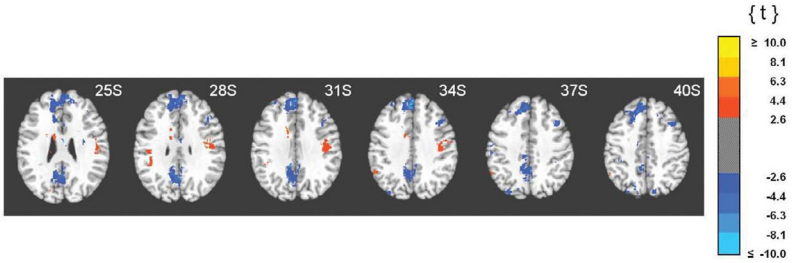

Fig. 3.

Clusters of unique correlations between fMRI activity and 0.05-0.099 Hz EEG spectral power. Functional images are displayed on the standardized average of 27 T1-weighted scans of a single participant known as the "Colin Brain" (Montreal Neurological Institute, Montreal, Canada). Voxel size is 1.0 mm^3.

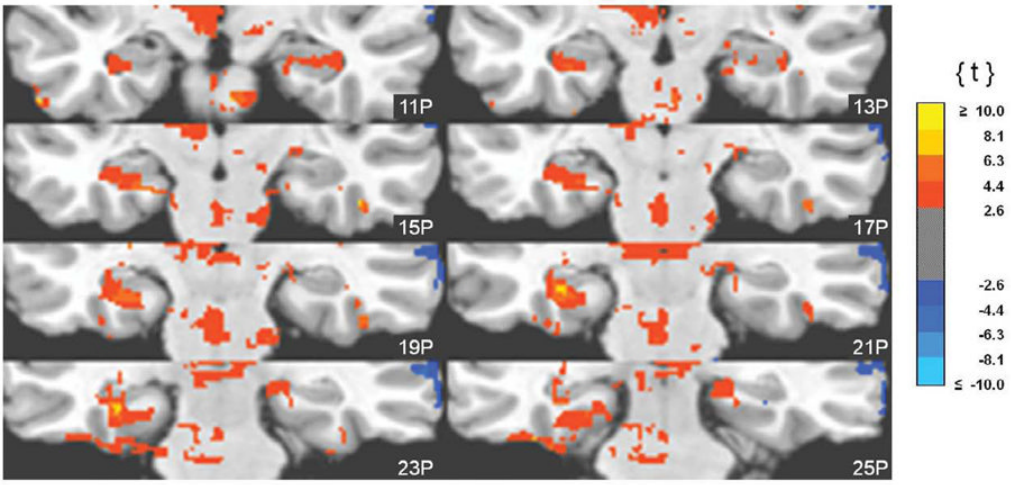

Fig. 4.

Clusters of unique correlations between fMRI activity and 0.05-0.099 Hz EEG spectral power. Functional images are displayed on the standardized average of 27 T1-weighted scans of a single participant known as the "Colin Brain" (Montreal Neurological Institute, Montreal, Canada). Voxel size is 1.0 mm^3.

Table 1

Average minutes of each EEG sleep stage across participants.

	M	SD
WAKE	9.64	6.21
1	10.50	8.06
2	35.03	30.52
3	17.63	18.41
4	13.09	18.67
REM	6.60	11.41
Total	92.50	54.15

Table 2

Clusters of unique negative correlations between fMRI activity and 0.05-0.099 Hz EEG spectral power.

Region of Interest	Cluster size (voxels)	Peak t score	x	y	z
Neocortex, Proisocortex (heteromodal)					
Medial Frontal Gyrus	15,465	−15.9	−6	38	28
Posterior Cingulate/Precuneus	5,116	−8.9	−4	−54	28
Superior Frontal Gyrus	4,587	−17.3	14	5	52
Precuneus	1,313	−5.8	16	−60	57
Middle Frontal Gyrus	893	−5.5	39	19	34
Middle Temporal Gyrus	853	−5.0	63	−16	−3
Middle/Superior Temporal Gyurs	846	−4.3	58	−39	11
Supplementary Motor Area	348	−4.7	−15	−11	58
Middle Frontal Gyrus	230	−4.1	45	44	5
Inferior Frontal Gyrus	204	−4.3	−42	39	8
Superior Parietal Lobule/Precuneus	165	−2.9	12	−77	40
Posterior Cingulate/Retrosplenial	162	−6.3	0	−40	18
Superior Parietal Lobule	145	−3.8	−18	−67	51
Superior Parietal Lobule/Precuneus	141	−6.4	−12	−79	42
Inferior Frontal Gyrus	141	−4.2	−49	27	3
Inferior Frontal Gyrus	120	−4.4	42	35	3
Middle Frontal Gyrus	104	−4.5	26	38	11
Middle Frontal Gyrus	103	−3.7	−29	44	33
Precuneus	103	−4.6	−13	−56	58
Supplementary Motor Area	100	−3.3	−12	−12	68
Neocortex (unimodal)					
Pre/Postcentral Gyrus	1,144	−4.7	−29	−28	57
Postcentral Gyrus	898	−9.5	9	−30	63
Postcentral Gyrus	760	−8.8	36	−37	51
Middle Occipital Gyrus	335	−3.9	−29	−77	37

Coordinates in Talairach space (Left/Right, Posterior/Anterior, Inferior/Superior negative/positive convention) were determined by the center of mass within the clusters of significant voxels from the final, masked dataset. Voxel size is 1.0 mm3. Clusters less than 100 voxels were excluded and correlations of note that are not included were Anterior Cingulate Cortex (89 voxels, t = 9.0, x = 2, y = −7, z = 26) and Postcentral Gyrus/Inferior Parietal Lobule (74 voxels, t = 3.6, x = −52, y = −24, z = 38).

Table 3

Clusters of unique positive correlations between fMRI activity and 0.05-0.099 Hz EEG spectral power.

Region of Interest	Cluster size (voxels)	Peak t score	x	y	z
Cerebellum					
Anterior Midline (Crus)	43,779	32.7	−6	−45	−20
Thalamus, Basal Ganglia, Brainstem					
Thalamus/Striatum/Midbrain	6,049	7.8	−8	−9	6
Pallidum	202	3.4	25	−5	2
Caudate (body)	122	3.7	−19	−21	23
Allocortex					
Hippocampus/Parahippo Gyrus	343	4.4	19	−24	−8
Neocortex (unimodal)					
Pre/Postcentral Gyrus	1,148	6.1	42	−15	30
Inferior Temporal Gyrus	1,119	12.5	−46	−39	−23
Inferior/Middle Temporal Gyrus	247	6.0	−32	1	−34
Fusiform Gyrus	332	6.8	−25	−89	−11
Middle/Superior Temporal Gyrus	159	4.7	43	−5	−10
Lingual Gyrus	153	4.2	−12	−92	−17
Cuneus	107	4.3	−7	−93	19
Neocortex (heteromodal)					
Gyrus Rectus	705	4.9	−6	21	−13
Supramarginal Gyrus	300	5.0	−40	−31	28
Inferior Frontal Gyrus	221	4.2	−48	14	3
Middle Temporal Gyrus	169	4.4	54	−33	−9
Temporal Pole	114	4.8	29	18	−32
Orbitofrontal Cortex	109	4.8	12	49	−13
Orbitofrontal Cortex	102	6.2	5	63	−3

Coordinates in Talairach space (Left/Right, Posterior/Anterior, Inferior/Superior negative/positive convention) were determined by the centers of mass within the clusters of significant voxels from the final, masked dataset. Voxel size is 1.0 mm^3. Clusters less than 100 voxels were excluded and correlations of note that are not included were Medial Thalamus (98 voxels, t = 4.1, x = −1, y = −24, z = 13), Ventrolateral Thalamus (33 voxels, t = 3.8, x = 20, y = −11, z = 13), and Parahippocampal Gyrus (39 voxels, t = 4.0, x = −13, y = −17, z = −22).